3D PRINTED SHORT CARBON FIBRES REINFORCED POLYAMIDE: TENSILE AND COMPRESSIVE CHARACTERISATION AND MULTISCALE FAILURE ANALYSIS

Andrea Canegrati [a], Luca M. Martulli [a], Gabriele Bolzoni [a], Milutin Kostovic [b], Gennaro Rollo [b], Andrea Sorrentino [b], Michele Carboni [a], Andrea Bernasconi [a]

a: Politecnico di Milano, Via La Masa 1, I-20156 Milano, Italy
andrea.canegrati@polimi.it
b: Polymer, Composites and Biomaterials Institute, National Research Council (CNR), Via Previati 1/E, 23900 Lecco (LC), Italy

Abstract: *The use of fused filament fabrication technology as a competitor of the conventional manufacturing processes for end-use parts production is of a great interest. However, a deep knowledge of the mechanical properties and failure behavior of printed parts is required to safely design final usable components. The present work aims to characterize the mechanical properties of a 3D printed short carbon fiber reinforced polyamide and to investigate the relationship between its unique morphology and its failure behavior. Tensile tests were conducted on rectangular specimens printed with an alternating sequence of layers with 0°/90° and ±45° raster orientation. Fracture surfaces of failed specimens were analyzed by Scanning Electron Microscopy (SEM). Possible failure mechanisms were then inferred by surface morphology analysis. Moreover, several specimens' geometries were designed and printed to characterize the in-plane and out-of-plane material compressive properties. Considerations about the longitudinal strength of the material were eventually drawn.*

Keywords: Fused Filament Fabrication; 3D printing; short fiber reinforced polymer; material characterization; failure analysis

1. Introduction

Fused Filament Fabrication (FFF), an extrusion-based 3D printing process, is nowadays one of the most common additive manufacturing technologies for Short Fiber Reinforced Polymers (SFRP).

There are major challenges related to the mechanical characterization of FFF printed composites. First, the manufacturing process induces anisotropy of the final part regardless the presence of the reinforcing phase. Testing FFF printed neat polymers parallel to the printing direction indeed allows for the highest mechanical properties to be achieved [1]. In addition to this, short fibers preferentially align with the filament's deposition direction, thus strengthen the neat polymer in longitudinal direction. Transverse mechanical properties appear to be governed by the intra-layer bond quality between adjacent filaments and inter-layer bonding between different layers. [1-2]. Then, there is a complex and conflicting dependence of the overall mechanical performance of the FFF printed component on both printing and material parameters. [1,3-4]. Finally, it is challenging to determine the actual cross section of specimens manufactured by FFF due to the large extent of voids and to the elliptical cross section retained

from the printed filaments. Thus, assuming a nominal cross section, the load carrying areas could be overestimated. [1]

Efforts of researchers were mainly focused on the optimization of printing parameters to achieve the highest performances of the final printed specimens. Material characterization plays a fundamental role as a baseline for developing models able to predict the mechanical properties of printed parts. However, an extensive investigation of the failure mechanism of FFF printed SFRP is still missing. This work aims to characterize the anisotropic properties of Onyx specimens obtained via FFF and investigate their failure mechanism under tensile and compressive quasi-static loads.

2. Materials and methods

2.1 Specimens fabrication

Test specimens were all produced via FFF technology by making use of a Markforged Onyx series printer. The material used to realize the specimens is a micro carbon fibre reinforced polyamide, whose tradename is Onyx, a micro-carbon fibres reinforced polyamide provided by Markforged [5]. The filament width and layer height were 0.4 and 0.1 mm, for all the printed specimens, respectively.

Tensile specimens were designed with a rectangular shape, which was 175 mm long and 30 mm wide. By stacking 32 layers, the specimens' thickness resulted to be 3.2 mm. This specimens' geometry was selected to avoid premature failure due to stress concentration at the fillet radii of dog-bone specimens, that might be caused by the printing pattern of the layer. [6] The Markforged's slicing software, namely Eiger, offers limited freedom in setting the printing parameters. It is prevented to print a unidirectional specimen using the software's default options. Because of this technological limitation, two sets of tensile specimens were printed with ±45° and 0°/90° stacking sequence of the layers.

Moreover, Eiger software requires the printing of a contour shell to envelope the part. Two concentric onyx rings were selected to this purpose. This results into lateral walls of the specimen's cross section that run parallel to the longitudinal axis of the specimens. A schematic layout of the tensile specimens is reported in Fig.1.

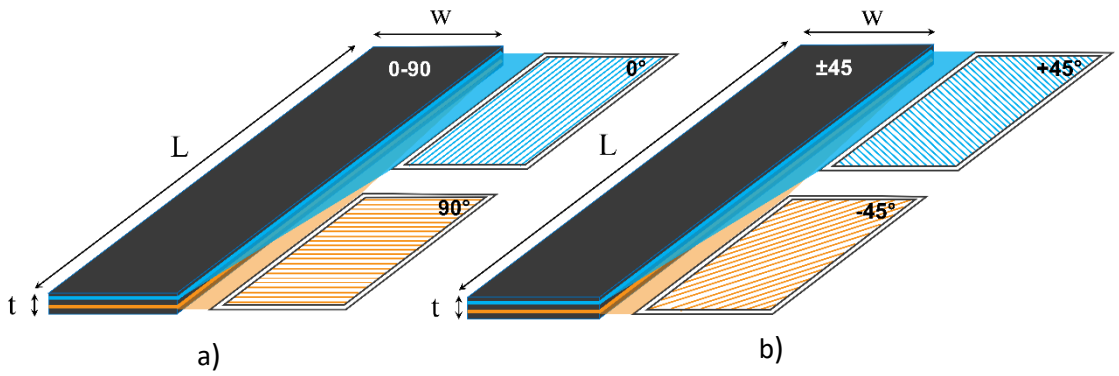

Figure 1. Schematic layout of the tensile specimens, a) 0°-90°, b) ±45° layers stacking sequence

Onyx end tabs, with dimensions of 50 mm x 30 mm x 2 mm, were separately printed by the same FFF printer used for the specimens. Tabs displayed an alternated sequence of layers with raster angles of ±45°. A low-cost, commercially available bicomponent epoxy resin glue was used to paste the tabs at the ends of the tensile specimens. The resulting gauge length of the specimens after the application of the tabs was 75 mm.

For the characterization of the in-plane compressive properties of the material, prismatic specimens were printed. Each specimen's layer is made up by fifteen concentric contours only, no infill was used. The printing pattern of a single layer is reported in Fig. 2, This led to stack layers displaying unidirectional filaments at 0°. The overall dimensions of the specimens were 12 mm wide, 30 mm high and 35 mm long as shown in Fig 2.a. Load aligns parallel to the 0° filaments.

Two types of specimens were printed to evaluate the out-of-plane material properties. One geometry was a hollow cylinder with outer diameter of 30 mm, and internal diameter of 15.6 mm. The other geometry was a hollow prism with square section, whose external and internal sides were 25 mm and 9 mm long, respectively. The height of both specimens' geometries was 10 mm. Each specimens' layer was made up by concentric contours only, as shown in Fig 2.b-c.

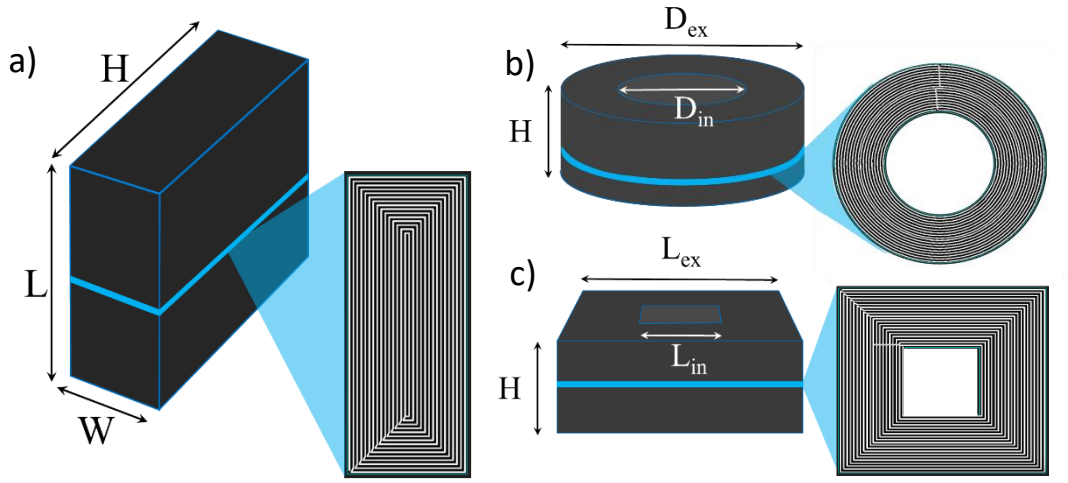

Figure 2. Schematic layout of the compression specimens: a) prism, b) hollow cylinder, c) hollow prism

2.2 Testing

Quasi-static tensile tests were performed according to ISO 527-4 [6]. Seven 0°/90° specimens and six ±45° specimens were tensile tested on an MTS Alliance RF testing machine. An extensometer was used to record the axial strains. A load ramp with a displacement rate of 0.75 mm/min (corresponding to 0.1 % of the specimens' gauge length) was first applied to the specimens up to 0.2 mm of axial displacement. This allowed an accurate evaluation of the Young's modulus of the specimens according to what prescribed in [6]. After the unloading of the specimens at the same speed, they were loaded up to failure at 5 mm/min of crosshead displacement rate.

Quasi-static compressive tests were carried out on two prismatic specimens, one hollow-prism and one hollow-cylinder. The specimens were tested on an MTS Alliance RF/150 to determine

the material's compressive properties. The compressive load was applied with a crosshead displacement rate of 0.2 mm/min.

2.3 Microscopy

The fracture surface of one tensile specimen per type was observed on a Zeiss EVO 50XVP Scanning Electron Microscope (SEM). The specimens' surfaces underwent a gold coating prior to scan, to enhance the quality of the images. Observation of the compressive tested specimens were carried out by an optical microscope.

3. Results

3.1 Tensile

Results of the tensile tests are shown in Fig.3 in terms of stress-strain curves. The values of the main mechanical properties obtained from testing are reported in Table 1.

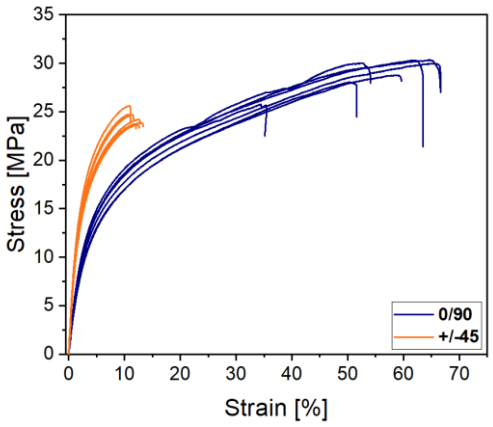

Figure 3. Stress-strain curves of tensile tested specimens

Table 1: Mean values and standard deviations of Young's modulus, tensile strength and strain at failure of tensile tested specimens.

	Young's modulus [MPa]	UTS [MPa]	Strain at failure [%]
±45	522 ± 37	29 ± 0.9	64.2 ± 9.2
0/90	967 ± 38	23.7 ± 0.6	11.8 ± 0.8

Specimens printed with 0°/90° raster angle displayed almost 85 % greater Young's modulus than the ±45° ones. Conversely, the strength of the ±45° specimens is about 22 % higher than that of the 0°/90° ones. According to what was reported in [8], the ±45° specimens failed for strains about 450% larger than that of the 0°/90° specimens, thus displaying a more ductile behaviour.

Moreover, the failure of the 0°/90° specimens occurred over a surface oriented at 90° with respect to the specimens' axis. Instead, the fracture surface of the ±45° specimens is oriented either at +45° or -45° in the infill region, whereas it tended to preserve the orientation of 90° (perpendicular to the filaments of the contour) in the wall regions.

3.2 Compression

Results of the compressive tests are shown in Fig.4 in terms of stress-strain curves. The values of the main mechanical properties obtained from testing are reported in Table 2.

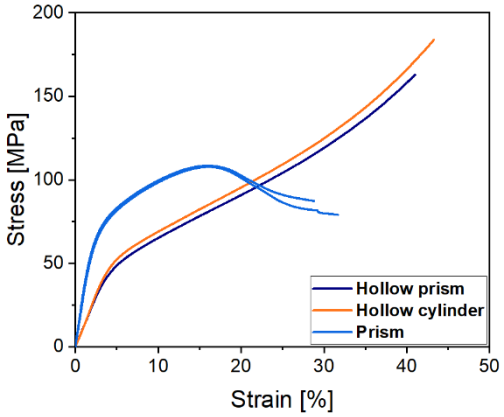

Figure 4. Stress-strain curves of tensile tested specimens

Table 2: Values of the compressive moduli and maximum compressive stress of the tested specimens.

	Out-of-plane		In-plane	
	Prism 1	Prism 2	Hollow prism	Hollow cylinder
Compressive modulus [GPa]	3.37	3.13	1.16	1.20
Max compressive stress [MPa]	108	108	-	-

Prismatic specimens allowed the evaluation of the compressive modulus of the material in the filament direction. It was found to be slightly greater than 3 GPa. The peak value of the stress in the filament direction was 108 MPa. Whereas two specimens' geometries were tested to evaluate the transversal moduli of the material. Good agreement existed between the resulting moduli, being 1.16 GPa and 1.20 GPa those obtained for the hollow-prism and the hollow-cylinder, respectively.

3.3 Fractography

Figure 5.a shows a SEM image of the fracture surface of a 0°/90° specimen. Two very different micromechanical behaviour of the material were inferred from the analysis of this fracture surface. A limited infill region experienced a micro-ductile failure mode. The matrix material of the filaments underwent large plastic deformation before failure, as clearly visible from the higher magnification images shown in Figure 5.b.

Conversely, micro-brittle failure occurred over an extended area of the specimen's cross section, including both walls and infill regions. The little to almost no plastic deformation of the filament's' matrix in those areas is highlighted in the close-up images of the filaments displayed in Figure 5.c and Figure 5.d.

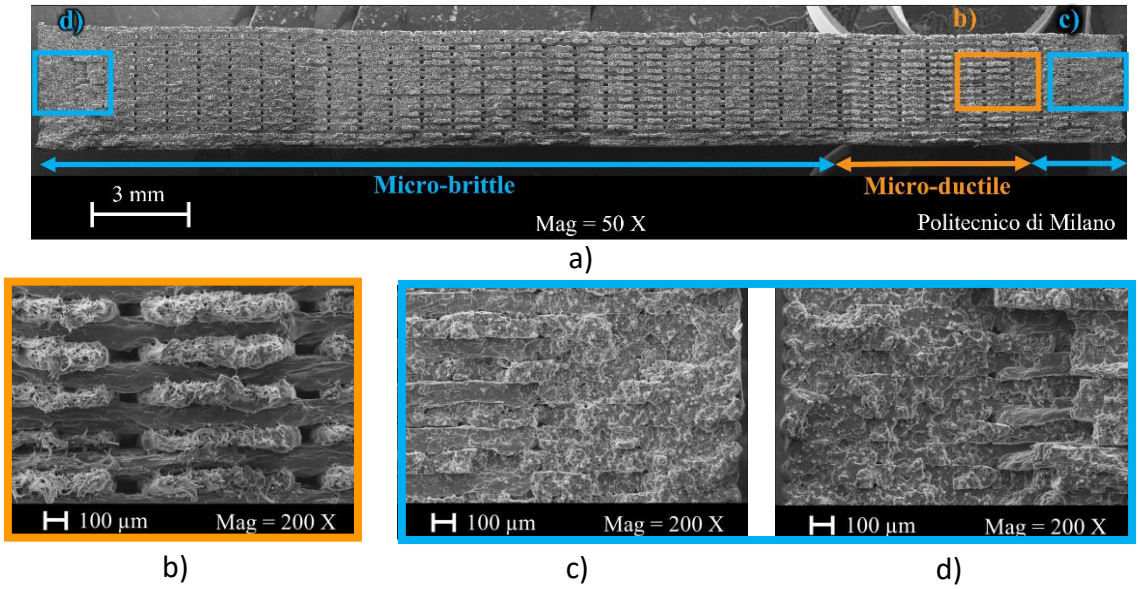

Figure 5. SEM images of: a) fracture surface of 0°/90° specimen, close up images 0 : b) micro-ductility of infill filaments, c-d) micro brittleness of the right and left walls respectively.

Figure 6.a displays a SEM image of the fracture surface of a ±45° specimen. The same micro-ductile and micro-brittle behaviour is observed. In the present case, the micro-ductile failure involved one of the two lateral walls and the filaments immediately adjacent to it. The large plastic deformation of this area is highlighted in Figure 6.b. The rest of the specimen's cross section displayed no evident plastic deformation, as shown in Figure 6.c.

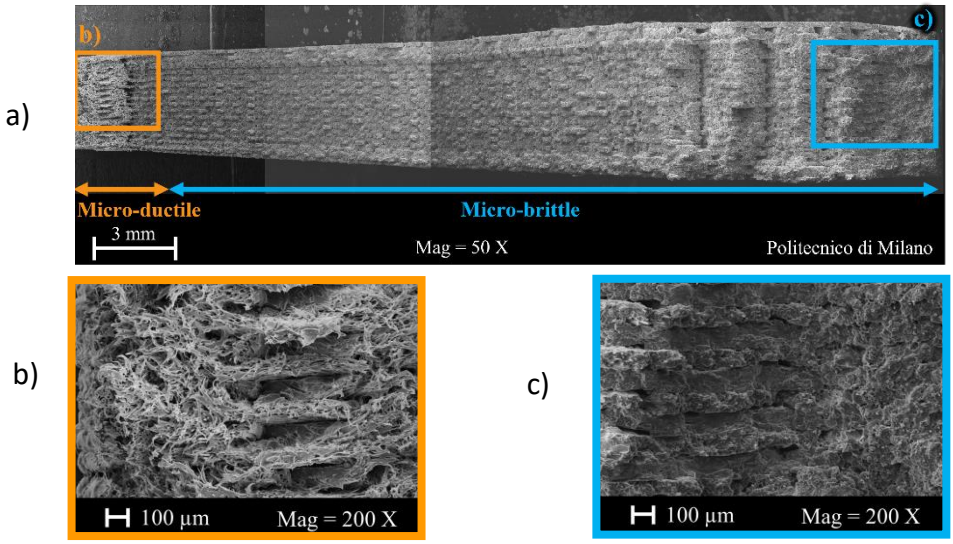

Figure 6. *SEM images of: a) fracture surface of ±45° specimen, close up images of: b) micro-ductility of left wall, c) micro brittleness of the right wall.*

A picture of the prismatic specimen tested under longitudinal compression is reported in Fig. 7.a. Shear bands formation and no evident inter-filaments debonding characterized the failure morphology of the prismatic specimens, as shown in the close-up images in Figure 7.a. Hollow prism and hollow cylinder specimens underwent barrelling, however no debonding between adjacent filaments was detected.

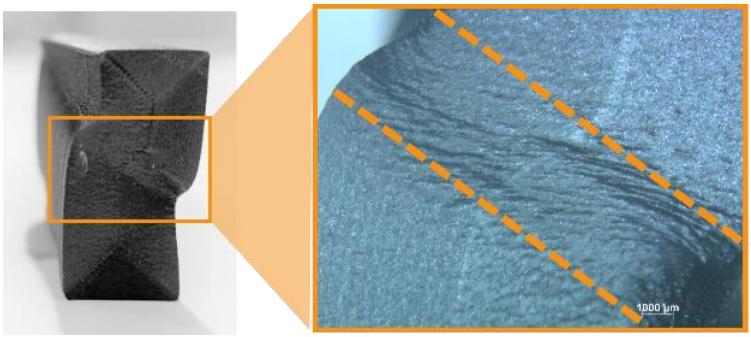

Figure 7. Failure morphology of the prismatic specimens under longitudinal load, close-up image of the shear bands.

4. Discussion

4.1 Tensile

The results of the tensile tests highlighted the influence of the raster orientation on both the stiffness and strength of the Onyx specimens printed via FFF technology. The higher stiffness of the 0°/90° specimens seemed to be mostly provided by the 0° filaments aligned with the load. By varying the angle between filaments and the load, as in the case of the ±45° specimens, the stiffness considerably decreases.

In contrast, the 0°/90° specimens appeared to fail at lower stress values than the ±45° ones. However, it is worth to mention that the strength values reported in Table 1 were obtained by diving the applied load by the nominal area of the cross section (initial width times initial thickness). Moreover, the SEM images of the fracture surface of the 0°/90° specimens evidenced an intra-filaments failure at 0° and an inter-filaments failure at 90° failure. This suggests that the effective resistant cross section is that provided by the 0° filaments only, thus lower than the nominal one. Therefore, the actual strength of 0°/90° specimens is most likely higher. Similar considerations can be applied to the strength of the ±45° specimens.

The onset of the specimens' failure might be associated to the micro-ductile areas of the specimens' fracture surface. There, large plastic deformation of the matrix most probably occurred at low strain rate. Once those regions have failed, a sudden failure of the remaining cross section yielded to the brittle failure of the rest of fracture surface.

4.2 Compression

Results of the compression tests highlight the anisotropic compressive behaviour of the FFF printed Onyx material. Longitudinal compression test of the prismatic specimens yielded to the highest mechanical properties. Seemingly the prismatic specimens did not fail for buckling.

Therefore, the maximum compressive stress obtained from testing could be assumed as a reliable estimation of the longitudinal compressive strength of the material. The transversal modulus seemed not to be influenced by the specimens' geometry used for the characterization. No sign of debonding between adjacent filaments were detected up to the maximum loads applied in the tests for all the tested specimens.

5. Conclusions

Mechanical characterization and failure analysis of an FFF printed short fibre reinforced polyamide were carried out. Results of tensile tests highlighted an effect of the raster angle on the mechanical properties of the printed specimens. Specimens printed with ±45° raster orientation were more compliant than those with 0°/90° raster orientation. The actual longitudinal tensile strength of the material could be underestimated by using the nominal cross-section. Failure of those specimens involved the filaments at 0° only, thus the effective resistant section is lower than the nominal one. The analysis of the fracture surface revealed that two different micro-mechanical behaviour were involved in the specimens' failure. The onset of the damage was confined in a limited portion of the cross-section, where large deformation occurred. Once this critical area fails, the remaining cross section fail at high strain rate, resulting in a micro-brittle failure behaviour.

Different in-plane and out-of-plane compressive properties resulted from the characterization of the Onyx material printed via FFF. The longitudinal compressive modulus was almost three times higher than the transversal one. The transverse modulus was not affected by specimens' geometry. The failure of unidirectional filaments longitudinally compressed occurred without buckling and debonding of adjacent filaments. Shear bands formation characterized the failed specimens' morphology. The maximum stress obtained by the test could be thus an accurate estimation of the compressive longitudinal strength of the material.

6. References

1. Brenken B, Barocio E, Favaloro A, Kunc V, Byron Pipes R, Fused filament fabrication of fiber-reinforced polymers: a review. Add Man 2018, 21:1-16.
2. Casavola C, Cazzato C, Moramarco V, Pappalettere C, Orthotropic mechanical properties of fused deposition modelling parts described by classical laminate theory. Materials & Design 2016,90:453-458.
3. Sanei SHR, Popescu D, 3D-Printed Carbon Fiber Reinforced Polymer Composites: A Systematic Review. J. Compos. Sci. 4, 98 (2020).
4. Krajangsawasdi N, Blok LG; Hamerton I; Longana ML., Woods BKS, Ivanov DS, Fused Deposition Modelling of Fibre Reinforced Polymer Composites: A Parametric Review. J. Compos. Sci. 5, 29 (2021).
5. Markforged, Onyx datasheet 2020: https://markforged.com/materials/plastics/onyx
6. Ahn S, Montero M, Odell D, Roundy S, Wright PK, Anisotropic material properties of fused deposition modelling ABS. Rapid Prototyping Journal 2002, 8(4):248-257.
7. EN ISO 527-4. Determination of tensile properties. 1997.
8. Jiang D, Smith DE. Anisotropic mechanical properties of oriented carbon fiber filled polymer composites produced with fused filament fabrication. Addit Manuf 2017;18:84–94.

